JOURNAL OF THERMOPHYSICS AND HEAT TRANSFER
Vol. 9, No. 4, October–December 1995

Comparison of Coupled Radiative Flow Solutions with Project Fire II Flight Data

David R. Olynick* and W. D. Henline†
NASA Ames Research Center, Moffett Field, California 94035-1000
Lin Hartung Chambers‡
NASA Langley Research Center, Hampton, Virginia 23681-0001
and
G. V. Candler§
University of Minnesota, Minneapolis, Minnesota 55455

A nonequilibrium, axisymmetric, Navier–Stokes flow solver with coupled radiation has been developed for use in the design of thermal protection systems for vehicles where radiation effects are important. The present method has been compared with an existing flow and radiation solver and with the Project Fire II experimental data. Good agreement has been obtained over the entire Fire II trajectory with the experimentally determined values of the stagnation radiation intensity in the 0.2–6.2 eV range and with the total stagnation heating. The effects of a number of flow models are examined to determine which combination of physical models produces the best agreement with the experimental data. These models include radiation coupling, multitemperature thermal models, and finite rate chemistry. Finally, the computational efficiency of the present model is evaluated. The radiation properties model developed for this study is shown to offer significant computational savings compared to existing codes.

Nomenclature

c_s = mass fraction for species s
e = total energy
e_v = vibrational energy
h_s = enthalpy of species s
I_{wall} = surface intensity
K_w = first-order reaction rate at wall
k = Boltzmann constant
m_s = mass of species s
p = surface pressure
Q_{rad} = source of radiation coupling
Q_{T-T_v} = source of translational–vibrational coupling
q = heat flux
q_c = total convective heat flux
q_r = radiative heat flux
q_{tj} = translational heat flux component
q_{vj} = vibrational heat flux component
T_d = characteristic temperature for dissociation
T_w = wall temperature
u_j = velocity component
V_{sj} = diffusion velocity component for species s
w_s = chemical source term for species s
x_j = direction component
γ = fraction of species s consumed at the surface
ρ = mixture density

Presented as Paper 94-1955 at the AIAA/ASME 6th Joint Thermophysics and Heat Transfer Conference, Colorado Springs, CO, June 20–23, 1994; received Aug. 15, 1994; revision received Feb. 2, 1995; accepted for publication March 9, 1995.

*Research Scientist, Reacting Flow Environments Branch. Member AIAA.
†Research Scientist, Reacting Flow Environments Branch. Senior Member AIAA.
‡Aerospace Engineer, Aerothermodynamics Branch. Senior Member AIAA.
§Assistant Professor. Member AIAA.

Introduction

A NUMBER of future NASA missions include scenarios where radiative heating may be important. For example, aerobraking scenarios use atmospheric drag in lieu of propulsive braking for trajectory manipulation. For aerobraking, it is believed that the contribution of radiation to the surface heating may be 50% or more of the total.[1] Another class of missions is planetary probes. For planetary probes, the reentry velocity is usually high enough to make radiation a significant or dominant heating mechanism. Therefore, to design an appropriate thermal protection system (TPS), accurate predictions of the magnitude of the incident radiation and its interaction with the flowfield and the vehicle's surface are needed. The major objective of this work is to develop a tool to aid TPS design for vehicles in which strong radiative effects are important.

To develop a prediction tool for re-entry flows where radiation is important, four major areas are addressed. First, a flow solver is needed that incorporates the appropriate physics of the flow such as chemical and thermal nonequilibrium and viscosity. Second, radiation properties such as emission and absorption coefficients for the various radiation mechanisms must be determined. Third, a radiation transport algorithm is needed to describe the interaction between the emitted photons and the fluid flow. Finally, accurate boundary conditions are needed to describe the interaction of the fluid and the radiation with the vehicle's surface. In this work, a two-dimensional or axisymmetric, Navier–Stokes flow solver that allows for chemical and thermal nonequilibrium is coupled with a detailed nonequilibrium radiation properties model that employs a tangent slab approximation for the radiation transport.

A heating analysis for the design of a vehicle's TPS generally requires determining a total heat load for re-entry. Calculating a total heat load requires heating estimates at a number of trajectory points. This leads to an emphasis on computational efficiency. Towards this end, an effort has been

made to select the most efficient numerical algorithms. For the flow solver, a modified version of Candler's nonequilibrium reacting gas code[2] is used to generate Navier–Stokes flow solutions. In this study, this code will be referred to as GIANTS (Gauss–Siedel implicit aerothermodynamic Navier–Stokes code with thermochemical surface conditions). To determine the radiation properties, a new radiation process model has been developed from the LORAN code of Hartung.[3] The algorithms employed in LORAN have been restructured, rewritten, and modified to achieve maximum computational performance on a vector supercomputer. The resulting algorithm has been designated as the nonequilibrium optimized vectorizable radiation process model (NOVAR). The two codes, GIANTS and NOVAR, have been coupled together to calculate flow solutions about the Project Fire II vehicle[4] for a number of points along the vehicle's trajectory. Numerical estimates of the heating and radiation intensity are compared with the experimental data and previously generated numerical solutions. Also, effects of thermal and chemical nonequilibrium are examined. Finally, the relative computational efficiency of the present algorithm is evaluated. Details of the methods are described in the following sections.

Procedure

Fluid Flow Governing Equations

The appropriate fluid dynamic equations for a re-entry flow have been described in a number of sources.[2,5–7] As a start, a set of equations was chosen that includes most of the important aspects of a re-entry flow in air. These equations include 11 species equations to determine the densities of N_2, O_2, NO, N, O, N_2^+, O_2^+, NO^+, N^+, O^+, and e^-, two total momentum equations, a total energy equation, and a separate energy equation for the vibrational energy. Solutions to this equation set for two-dimensional and axisymmetric flows are obtained using the Gauss–Seidel procedure of Candler and MacCormack.[2,8]

In this work, the thermal model was developed assuming that the translational temperature is equal to the rotational temperature and that one vibrational temperature is representative of all the vibrational modes of the gas mixture. The energy equations used to describe this model are as follows. The total energy equation is given by

$$\frac{\partial(\rho e)}{\partial t} + \frac{\partial[(\rho e + p)u_j]}{\partial x_j} + \frac{\partial(u_i\tau_{ij} + q_{tj} + q_{vj})}{\partial x_j} + \frac{\partial\left[\sum_s^{nsp}(\rho_s h_s V_{sj})\right]}{\partial x_j} = -Q_{\text{rad}} \tag{1}$$

The vibrational energy equation is

$$\frac{\partial(\rho e_v)}{\partial t} + \frac{\partial(\rho e_v u_j)}{\partial x_j} + \frac{\partial\left(q_{vj} + \sum_s^{\text{dia}} \rho_s e_{vs} V_{sj}\right)}{\partial x_j} = \sum_s^{\text{dia}} w_s e_{vs} + Q_{T-T_v} \tag{2}$$

where $w_s e_{vs}$ is the vibrational energy lost or gained from chemical reactions. The coupling between the vibrational and translational modes Q_{T-T_v} is modeled using a Landau–Teller formulation. The relaxation times for the vibrational modes are obtained from Millikan and White.[9] Radiation coupling enters the equations through the source term Q_{rad} in the total energy equation. In this study, the contribution of the electronic modes to the total energy and the radiative source of vibrational energy is neglected. For the radiation calculation, it is assumed that the electronic temperature is equal to the vibrational temperature. This approximation greatly simplifies the computational effort. At the Fire II conditions where vibrational–electronic coupling and molecular chemistry effects are important, this assumption may be a reasonable approximation.

The chemical source terms are modeled using the Park 1993 rates.[10] However, for electron impact ionization, the rates deduced by Wilson[11] are employed. Also, the ionization rates are assumed to be a function of the translational temperature T. Ideally, these rates should be a function of the free electron temperature. Thus, this assumption should be applied with caution. In the region of thermal nonequilibrium within the shock, $T_d = \sqrt{TT_v}$ is used as the controlling temperature for the dissociation rates.

The mixture rules for the viscosity and translational and vibrational conductivity used in this work are based on the formulations of Gupta et al.[5,12] The cross section data by Yos in Refs. 5 and 12 has been reviewed and updated to improve the collision modeling.[13] The multicomponent diffusion coefficients are treated using a bifurcation approximation.[14,15]

Radiation Coupling and Transport

In the Gauss–Seidel method, the chemical, inviscid and viscous terms are treated in an implicit manner. With the addition of radiation, a method of treatment, implicit or explicit, must be selected for the radiation source term Q_{rad}. Gökçen treated the radiation source term in an implicit manner using the Gauss–Seidel method.[16] He found that an implicit treatment of the radiation source greatly increased the computational costs and reduced the stability of the overall method. For a detailed radiation model, the application of the method was limited to inviscid flows because of the increased computational cost. Thus, in the current work, the radiation is treated in a loosely coupled manner.

The loosely coupled treatment of the radiation source has been described by Hartung et al.[3] The application of the loosely coupled method involves a number of steps. First, a converged flow solution is generated without radiation. The converged flow solution is then used to produce an initial estimate of the radiation field. Next, the flow code is run for a certain number of iterations with the radiation field fixed. Then, the radiation field is updated using the new flow solution. This procedure continues until the flow and radiation solutions converge.

The radiation transport is modeled using a one-dimensional tangent slab approximation. In the tangent slab model, radiation properties are assumed to vary only in one dimension. Perpendicular to the direction of variation, radiation properties are assumed constant in planes that extend to infinity. For Fire II, tangent slab is a reasonable approximation in the stagnation region because of the highly blunted shape of the forebody. Most of the variation in flow properties occurs in the direction normal to the surface of the vehicle.

Radiation Properties

The radiation properties model employed in this study is a derivative of the Langley optimized radiative nonequilibrium code (LORAN).[17,18] LORAN generates absorption and emission coefficients for the following radiative processes: atomic bound–bound, bound–free and free–free transitions for N and O and the N_2^+ first negative, N_2 first and second positive, and Lyman–Birge–Hopfield, NO β and γ, and O_2 Schumann–Runge molecular band systems. The various atomic and molecular excited state populations are calculated using the quasi-steady-state (QSS) approximation of Park.[19]

When LORAN was developed, a major goal was to couple the method with a flowfield solver. The most sophisticated nonequilibrium radiation solver available is the NEQAIR code of Park.[20] The NEQAIR code calculates the radiation properties for the atomic and molecular processes listed in the

previous paragraph using a detailed line-by-line approach. This detailed approach was deemed too costly for flow coupling. Thus, a number of approximations were made to improve the computational efficiency of the method.

The major differences between NEQAIR and LORAN are that the radiation properties for the molecular band systems are calculated using a "smeared band" approximation instead of the line-by-line approach used in NEQAIR, and an optimized spectral array is generated to reduce the total number of spectral points.[21] Thus, the accuracy of the method is considered less than the detailed line-by-line approach of the NEQAIR model. However, the absorption and emission coefficients generated by the LORAN code have been shown to be comparable to those generated from the NEQAIR code of Park.[17]

Although the computational cost of the LORAN method is lower than that of NEQAIR and the feasibility of using the method in coupled calculations has been demonstrated, the computational cost to couple LORAN with a flow solver is still large.[3] Initial timing tests on LORAN demonstrated that large portions of the code were nonvectorized. The low computational efficiency of the method was the major impetus for the development of the NOVAR algorithm. Timing comparisons between NOVAR and LORAN are presented in the results section.

The physical modeling of the various radiation mechanisms in LORAN and NOVAR are similar. However, to maximize the level of vectorization, the implementation of these models in the codes is quite different. A description of the algorithmic differences between LORAN and NOVAR are described in Ref. 15.

One major difference between NOVAR and LORAN is the method used to calculate the populations of the excited molecular and atomic states. In LORAN, a QSS approximation is employed to determine the populations of these states. In NOVAR, the QSS distribution is replaced by a Boltzmann distribution, which while theoretically not totally correct for the nonequilibrium region, may be adequate for the Fire II flight regime.

In the course of developing the NOVAR algorithm, it was found that if an identical flow solution and excited state population distribution were used as an input for both NOVAR and LORAN, then the differences between the calculated radiation properties were small. Figure 1 shows calculated absorption and emission coefficients from NOVAR and LORAN using equilibrium air at a pressure of 2 atm and a temperature of 10,000 K employing a Boltzmann distribution for the excited states. These conditions are representative of the flow behind the shock for Fire II near peak heating. It can be seen in the figure that the percent difference between the calculated emission coefficients is on the order of 2–3% or less. The radiation properties were generated at different spectral locations. Thus, some of the differences result from interpolating the emission coefficients onto an identical frequency distribution for the comparison. A similar result was obtained for the absorption coefficient.

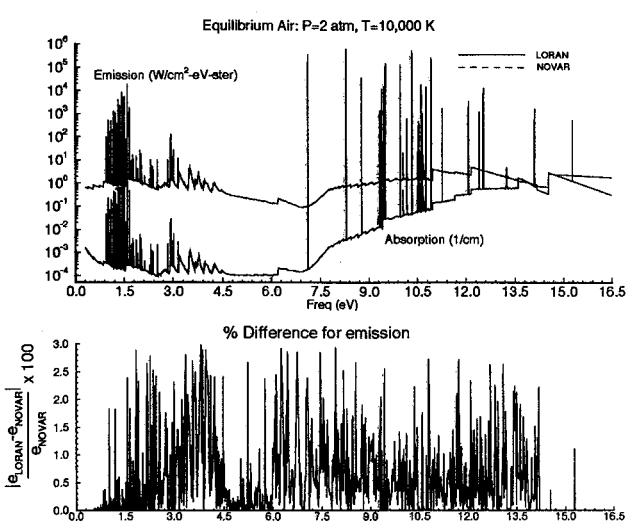

Fig. 1 Comparison of absorption and emission coefficients for equilibrium air conditions.

Boundary Conditions

For this study, no-slip conditions are assumed. Thus, the velocity at the surface boundary is zero. The wall temperature is assumed to be constant, which is appropriate for the essentially "cold wall" of the Fire II experiment. Therefore,

$$U_s = U_w = 0 \qquad T_s = T_w \tag{3}$$

where the subscripts s and w denote properties at the computational boundary and wall.

For radiation, the wall is assumed to emit radiation as a blackbody at the specified wall temperature. The actual Fire II vehicle surface was nonblack. However, because of the low surface temperature, inaccuracies in this assumption are assumed small. In the freestream, the radiation flux is neglected, i.e., precursor effects are ignored.

For chemistry, the wall is assumed to be fully catalytic to the ions and noncatalytic to the neutral species. Therefore, for the ions, the mass flux at the wall is related to the rate of diffusion towards the surface as follows[6]:

$$\left(\rho D \frac{\partial c_s}{\partial \eta}\right)_w = (\rho_s K_s)_w = w_{sw} \tag{4}$$

where η denotes the direction normal to the surface. The reaction rate at the wall is given by

$$K_{ws} = \gamma_s \sqrt{(kT_w/2\pi m_s)} \tag{5}$$

where γ_s is the fraction of species s consumed at the surface, k is the Boltzmann constant, and m_s is the mass of species s.

For the Project Fire II experiment, the heat plug containing the thermocouples was constructed out of beryllium.[4] Beryllium is highly catalytic to reactions. Thus, a fully catalytic wall boundary condition has been assumed by many researchers when simulating the Fire II experiments.[21,22] However, with the presence of atomic oxygen in the flow, it is likely that the surface of the beryllium was highly oxidized. In general, the catalytic potential of a material is related to its electrical properties. Materials with a high electrical conductance such as metals usually act as catalysts for reactions. Conversely, materials with a low electrical conductance, such as insulators, are poor catalysts.[23] Beryllium oxide has an extremely low electrical conductance and behaves as an insulator. Thus, in this work, the wall is assumed to be noncatalytic to reactions involving neutral species and γ_i for neutrals in Eq. (5) is set to zero. For the ions, the wall is assumed to be electrically uncharged. Thus, any ion reaching the surface is neutralized.[6] Therefore, the wall is considered fully catalytic to ions and $\gamma_{\text{ions}} = 1$.

Results

The major objective of this study is to develop a coupled radiation solver for TPS design. To achieve this objective, a number of topics are discussed in this section. First, to assess the nonequilibrium flow modeling employed in GIANTS, an axisymmetric flow solution for the Project Fire II 1634-s conditions is generated and compared with results from the LAURA code of Gnoffo.[5] These flow calculations are used to generate uncoupled stagnation line radiation solutions using NOVAR. Next, a baseline heating calculation is carried out over the Fire II trajectory using GIANTS/NOVAR. At

Table 1 Fire II trajectory conditions

Time, s	Altitude, km	Velocity, km/s	Density, kg/m^3	T_∞, K	T_w, K
1634	76.42	11.36	3.72×10^{-5}	195	615
1636	71.04	11.31	8.57×10^{-5}	210	810
1637.5	67.05	11.25	1.47×10^{-4}	228	1030
1639	63.11	11.14	2.41×10^{-4}	242	1325
1640.5	59.26	10.97	3.86×10^{-4}	254	1560
1643	53.04	10.48	7.80×10^{-4}	276	640
1644	50.67	10.19	1.02×10^{-3}	281	1100
1645	48.37	9.83	1.32×10^{-3}	285	1520
1648	42.14	8.30	3.00×10^{-3}	267	1560
1651	37.19	6.19	6.05×10^{-3}	253	1060

each trajectory point, uncoupled and coupled radiative forebody flow solutions are generated. Then, numerically determined values of the stagnation radiative intensity and the stagnation heat transfer are compared with the Fire II experimental data and numerical results using LAURA/LORAN. With a baseline established, the effects of a number of flow assumptions are examined. Radiative flow solutions are generated with GIANTS/NOVAR assuming thermal equilibrium, and thermal and chemical equilibrium. Stagnation point results are compared with the experimental data and the baseline calculations. Finally, the computational efficiency of the present method is described.

The flight conditions considered in this work are listed in Table 1.[4] Progressing from 1634 to 1651 s, these conditions represent nonequilibrium to equilibrium flow conditions. Experimentally measured values for the stagnation radiation intensity in the 0.2–6.2-eV range and total stagnation heating were extracted from plots contained in Refs. 4 and 24. In Ref. 25, the accuracy of the radiation data from the flight experiment was assessed and the data points were classified as prime or nonprime. Prime data points are considered to be the most accurate, i.e., where the flow was free of any contaminants. The Fire II flight experiment was composed of layers of beryllium and asbestos and the radiation sensor had a quartz window. For the nonprime points, it was believed the flow was contaminated or the quartz window was nearing its melting point. Thus, the radiation data at these points are not considered to be as accurate as at the prime data points.

For all the GIANTS calculations in this work, grids with 80 cells normal to the body and 37 cells along the body were employed. In past work, it was determined that this resolution was adequate.[26] The accuracy of this grid resolution including the normal spacing distribution is discussed in Ref. 26.

Comparisons with LAURA

For the first set of calculations, the nonequilibrium aspects of the present code are assessed. The amount of radiation emitted in the flowfield is directly proportional to the number of particles in each of the excited atomic and molecular states. The populations of these states are a function of the species densities and the vibrational and electronic temperature. In GIANTS, the electronic energy of the various species is neglected and the electronic temperature is assumed equal to the vibrational temperature for the radiation calculation. Thus, any of the flow mechanisms that affect the vibrational temperature can have a strong influence on the radiation calculation. Two flow mechanisms that strongly influence the vibrational temperature are the controlling temperatures used in dissociation and electron impact ionization. In GIANTS, the forward dissociation rates are assumed to be a function of the vibrational and translational temperatures and the electron impact ionization reactions are assumed to be a function of the translational temperature. To illustrate the effects of these models on the flow and radiation calculations, a numerical solution for the 1634-s trajectory point is considered. For comparison purposes, a flow solution without coupled radiation from GIANTS is contrasted with a solution generated from LAURA. In LAURA, the vibrational and electronic modes are assumed to be a common energy pool characterized by one temperature T_{ve}. The dissociation rates are assumed to be a function of the translational and vibrational–electronic temperatures and the electron impact ionization rates are assumed to be a function of the vibrational–electronic temperature.

In Fig. 2, temperature profiles along the stagnation streamline are compared from GIANTS and LAURA. It can be seen in the figure that LAURA predicts a much higher translational temperature in the nonequilibrium portion of the flow. Both methods predict a similar equilibrium temperature behind the shock. The major reason for the large differences between the nonequilibrium temperatures is the treatment of electron impact ionization. In LAURA, using T_{ve} as the controlling temperature in the electron impact ionization rates lowers the amount of ionization, which leaves more energy in the translational modes. The vibrational–electron–electronic temperature is increased via translational–vibrational and translational heavy particle-free electron coupling, which leads to an overshoot of the vibrational–electron–electronic temperature behind the shock. In GIANTS, using T as the controlling temperature in the electron impact ionization rates increases the amount of ionization, which lowers the translational temperature. The effect of using different rate controlling temperatures on the species densities is illustrated in Fig. 3, which shows the nitrogen species, N_2, N, N_2^+, and N^+ along the stagnation streamline. The faster rate of N^+ ion

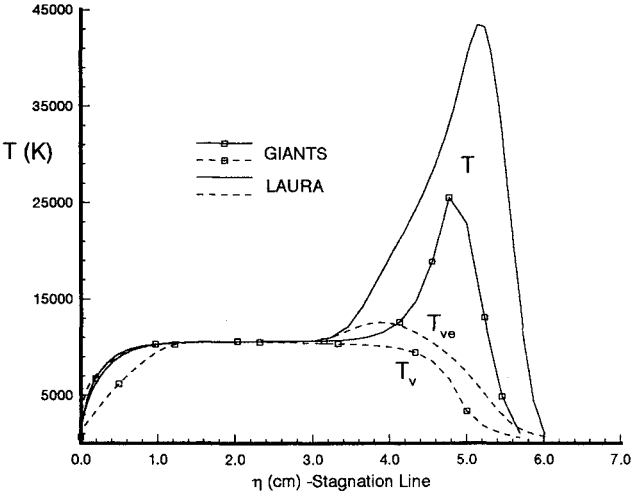

Fig. 2 Temperatures along the stagnation line for 1634-s, axisymmetric flow.

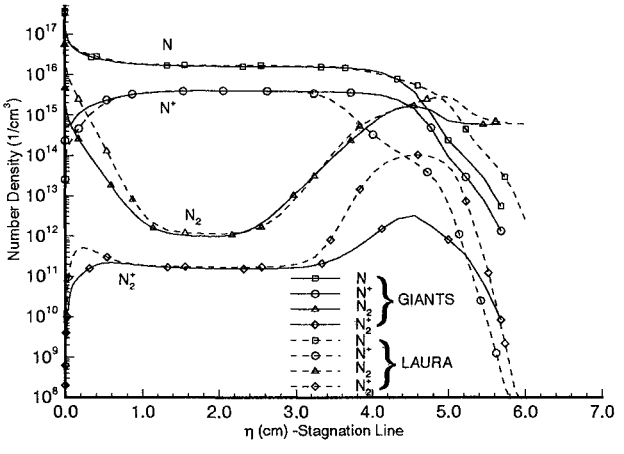

Fig. 3 Nitrogen species along the stagnation line for 1634 s.

production is clearly shown for GIANTS. Also, it can be seen that LAURA predicts a much higher N_2^+ concentration in the nonequilibrium portion of the flow. The larger N_2^+ density for LAURA results from the high nonequilibrium translational temperature, which promotes charge exchange reactions that produce N_2^+. In the region of thermal equilibrium behind the shock, both methods predict similar nitrogen species concentrations. Near the surface differences in the species densities can be attributed to the wall catalysis boundary conditions employed in the methods. A noncatalytic wall for the neutrals is assumed in GIANTS, while a fully catalytic wall for all species is assumed in LAURA.

The effects of the nonequilibrium flow modeling on the radiation calculations are illustrated in Figs. 4 and 5. Uncoupled stagnation line radiation solutions are generated from the GIANTS and LAURA flow solutions using NOVAR. Figures 4 and 5 show the radiative flux q_r away from the wall and toward the wall along the stagnation line. In the tangent slab approach, the net radiative flux is the difference between the flux towards and the flux away from the wall. First, it can be seen that the radiative flux generally follows T_v and T_{ve}. In Fig. 4, the radiative flux away from the body rises as the vibrational temperature increases and levels off at the shock as the temperature drops. The overshoot in T_{ve} for the LAURA calculation leads to an overshoot in the radiative flux. In Fig. 5, the radiative flux toward the body quickly increases as T_v and T_{ve} rise. Nearest the wall, the radiative flux drops slightly with temperature as the result of absorption in the thermal boundary layer.

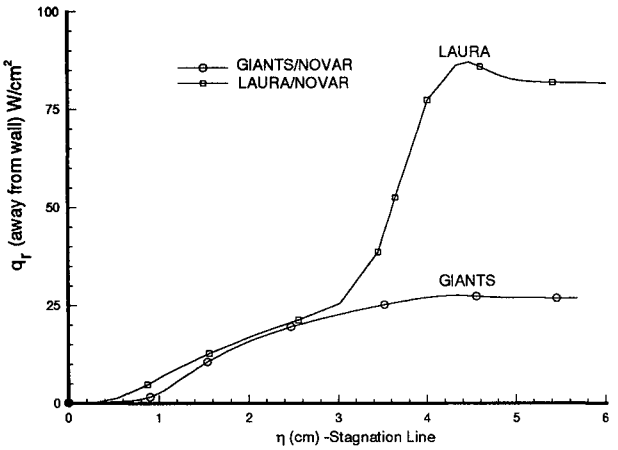

Fig. 4 Radiative flux away from the wall along the stagnation line for 1634 s.

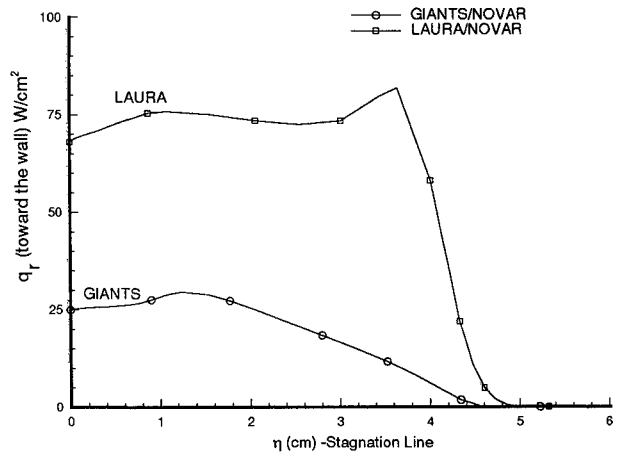

Fig. 5 Radiative flux toward the wall along the stagnation line for 1634 s.

Table 2 Comparison of radiative intensities for Fire II 1634 s

	I_{wall}, 0.2–16.5 eV, W/cm^2-sr	I_{wall}, 0.2–6.2 eV, W/cm^2-sr	q_{wall}, W/cm^2
Experiment	—	1.3 ± 20%	—
LAURA/NOVAR	12.8	4.2	67.9
GIANTS/NOVAR	4.7	1.4	24.8

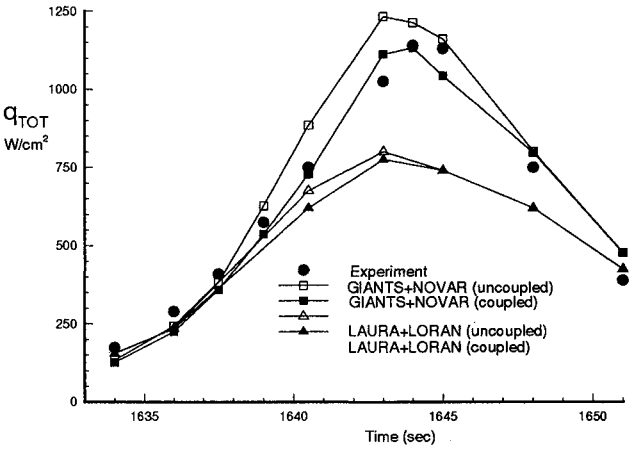

Fig. 6 Comparison of total stagnation heating down the Fire II trajectory.

The higher radiative flux for LAURA results mostly from two radiation mechanisms, atomic line and molecular N_2^+. The higher nonequilibrium T_{ve} profile increases the populations of the higher electronic states of N and O, which results in more atomic line radiation. A secondary effect is molecular radiation from N_2^+, which is a strong radiator. As shown in Fig. 3, the density of N_2^+ is much larger for LAURA than for GIANTS in the shock region. Thus, the higher N_2^+ density and larger T_{ve} profile increase the molecular radiative flux.

Numerical and experimental surface radiation intensities and heating values for the two uncoupled flow solutions are summarized in Table 2. In the experiment, the stagnation radiation intensity in a frequency range between 0.2–6.2 eV was measured. The experimental value for 1634 s was 1.3 W/cm^2 with an error range of ±20%. The uncoupled surface intensities generated from the LAURA solution overpredict the experimental surface intensity in the sensor range by a factor of about three. The intensity value generated from GIANTS is in good agreement with experimental data. The LAURA calculation also produces a much higher fraction of uv radiation. This radiation comes primarily from atomic lines in the shock. Although some of this radiation is self-absorbed, a significant portion is transported in the wings of the atomic lines,[27] which results in a higher radiative surface heating value.

Trajectory Calculations

With a baseline for comparison established between the GIANTS and LAURA flow codes, coupled radiative calculations using GIANTS/NOVAR are carried out over the entire Fire II trajectory. Numerically determined values for the uncoupled and coupled total stagnation heating values and radiative intensities are compared with the Fire II experimental data and with numerical values obtained using LAURA/LORAN. The LAURA/LORAN data were extracted from plots published in Ref. 21. Figure 6 is a comparison of the experimental total stagnation heating (convective and radiative) along the Fire II trajectory with uncoupled and coupled radiation solutions using GIANTS/NOVAR and LAURA/LORAN. The total stagnation heating is composed of the convective contribution and the radiation absorbed into the

surface accounting for the absorption properties of beryllium. It can be seen that there are large differences between the predicted heating values from the methods. In the early portions of the trajectory both methods underpredict the total heating. It appears from 1634–1637.5 s that both methods are in good agreement. However, a fully catalytic wall boundary condition is assumed for LAURA, while a noncatalytic boundary condition for the neutrals is assumed for GIANTS. If identical boundary conditions were used for both methods, then the heating would be much higher for the GIANTS solution in the early part of the trajectory and the discrepancies between the methods would be larger. If the surface of the vehicle was only partially oxidized, then assuming a small finite catalytic boundary condition for the neutrals in GIANTS would improve the agreement with the early part of the flight experiment. Near peak heating, the coupled GIANTS solution tracks the experimental data fairly well. The LAURA results underpredict the data. It can be seen for the GIANTS results that coupling the radiation with the flow improves the agreement with the experimental data by lowering the amount of radiative heating. This effect is illustrated in Fig. 7.

Figure 7 shows a comparison of the measured and predicted stagnation intensity in the 0.2–6.2-eV range. The solid circles denote prime data points where the experimental data were considered to be most accurate. It can be seen in the figure that predicted intensity values from GIANTS/NOVAR are in good agreement with the experimental data near the prime data periods. In the 1643–1648-s time period, the GIANTS solution overpredicts the radiation intensity. However, the accuracy of the radiation data in this period is suspect. Further, the agreement of GIANTS with the total heating in this period was good. The LAURA/LORAN combination overpredicts the radiation at 1634 s and underpredicts the radiation near its peak at 1643 s. However, agreement with the experimental data is good in the 1643–1648-s time period overpredicted by the present method. It can be seen for both methods that radiation coupling lowers the amount of radiation. As expected, the coupling effects are largest where the radiation intensity is largest. Discrepancies between the GIANTS/NOVAR and LAURA/LORAN solutions could be the result of the different nonequilibrium models employed in both LAURA and GIANTS, as previously demonstrated. Another factor could be the QSS distribution that is employed in the LORAN code. Some effects of the QSS approximation on the radiation calculation are examined in Ref. 15.

Figure 8 shows a comparison of the convective heating predicted by GIANTS and LAURA along the flight trajectory. Experimental data were not available for the convective heating. It can be seen that large differences exist in the convective

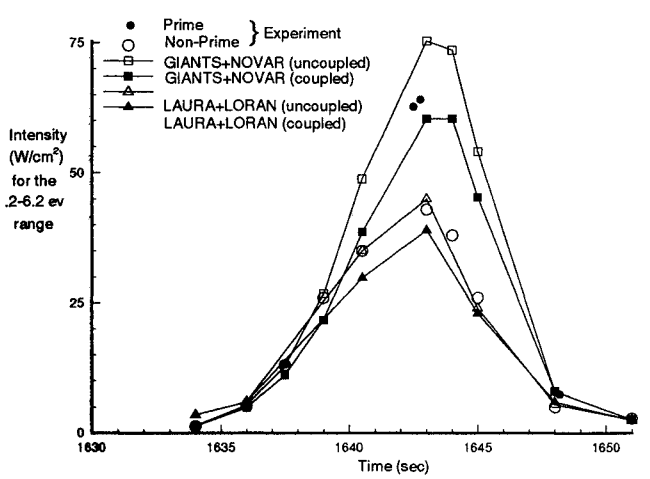

Fig. 7 Comparison of stagnation intensities down the Fire II trajectory.

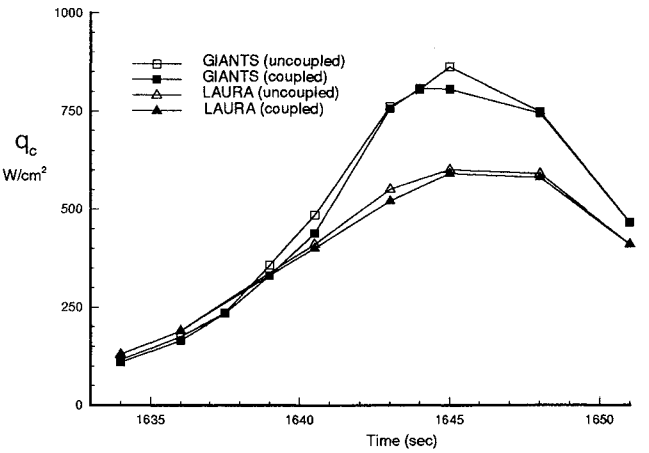

Fig. 8 Comparison of convective heating down the Fire II trajectory.

heating predicted by both methods. Some of the discrepancy can be attributed to differences in the diffusion models employed in GIANTS and LAURA. However, these differences are magnified by the fact that different catalytic boundary conditions were used for both LAURA and GIANTS and that radiation coupling had only a small effect on the convective heating. The largest differences occur at peak heating.

Nonequilibrium Modeling Effects

In the previous set of calculations a stagnation heating analysis was generated for the Fire II trajectory using a set of nonequilibrium models that included a two-temperature thermal model and finite rate chemistry. Using these models in GIANTS/NOVAR, a favorable comparison was obtained with the Fire II experimental data. In the next set of calculations, simpler models are used to describe the nonequilibrium aspects of the flow. Coupled radiative calculations are generated using GIANTS/NOVAR assuming a one-temperature thermal model with finite-rate chemistry and assuming a one-temperature thermal model and chemical equilibrium. These flow solutions were carried out to determine if less complex flow modeling could be used over all or part of the Fire II trajectory and still yield satisfactory agreement with the experimental data.

In GIANTS, the effects of a one-temperature thermal model are simulated by decreasing the relaxation time between the vibrational and translational modes by a factor of 3000. To simulate thermal and chemical equilibrium, the vibrational relaxation times are decreased by a factor of 3000 and the chemical rates are increased by a factor of 1000. Flow solutions using a simulated one-temperature thermal model and simulated equilibrium are generated with and without radiation for three trajectory points, 1634, 1643, and 1651 s. These trajectory points represent nonequilibrium, near-equilibrium, and equilibrium flow conditions.

Figure 9 is a comparison of total stagnation heating for the one-temperature, equilibrium, and previous nonequilibrium calculations with the Fire II experimental data. The total heating predicted by the one-temperature and equilibrium formulations is higher than the nonequilibrium formulation and the experimental data at each of the three calculated trajectory points. A one-temperature thermal model increases the total heating because the translational–rotational–vibrational temperature overshoots the postshock temperature. The increased temperature leads to an increase in the radiative heating. The equilibrium model increases the heating because the faster chemical rates in the cold boundary layer increase the rate of atomic recombination, which raises the translational temperature. The increased translational temperature leads to higher convective heating. These effects are illustrated in Figs. 10–13.

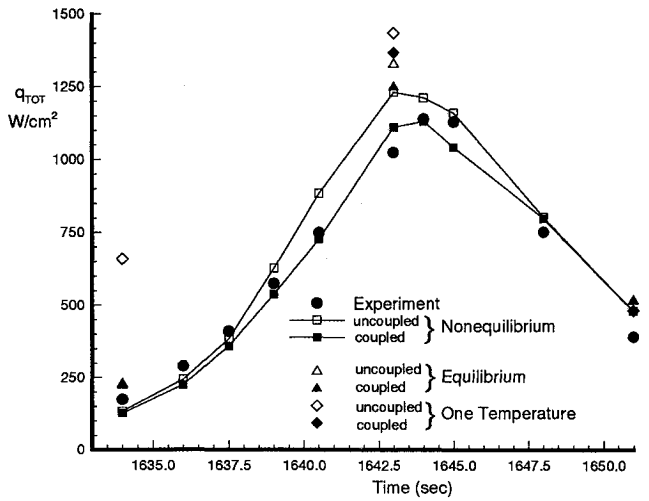

Fig. 9 Effects of thermal and chemical equilibrium on the stagnation heating along the Fire II trajectory.

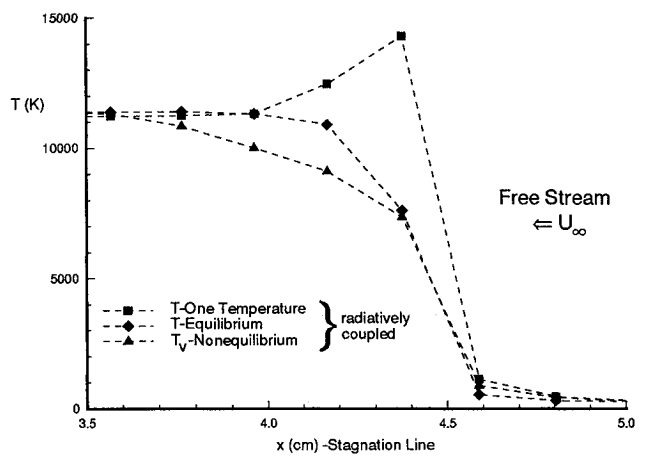

Fig. 10 Vibrational and total temperatures in the shock region for the 1643-s conditions.

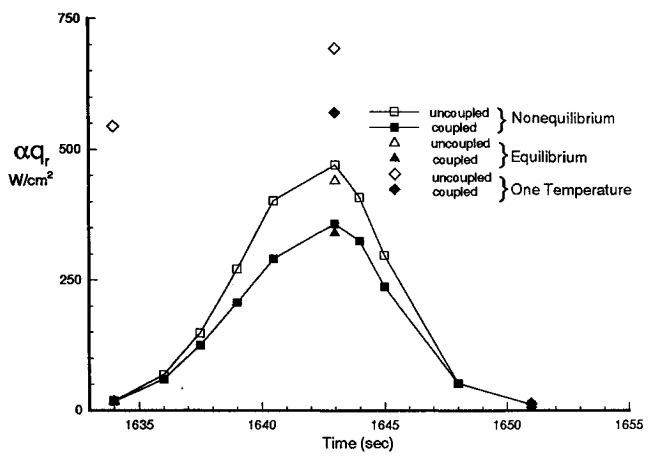

Fig. 11 Effects of thermal and chemical equilibrium on the absorbed radiative heating.

Figure 10 is a plot of the vibrational temperature and the translational–rotational–vibrational temperature in the shock region for the 1643-s conditions. It can be seen that a one-temperature model overshoots the postshock temperature that all three formulations approach. As previously described in Figs. 3–5, an overshoot in the vibrational temperature can produce a large increase in the radiative flux. The overshoot for the one-temperature model is the result of chemical non-equilibrium in the shock region. This result was also observed for the 1634-s conditions. At the 1651-s conditions, the flow is near chemical equilibrium in the shock and all three models yield similar temperature profiles. In contrast, the equilibrium temperature is much closer to the nonequilibrium vibrational temperature that was observed at all three trajectory conditions.

Figure 11 shows the radiative heating absorbed by the beryllium surface for all three formulations. As expected, a one-temperature thermal model results in a significantly larger absorbed radiative flux at the 1634- and 1643-s conditions. The uncoupled radiative flux was so large at the 1634 s conditions that a coupled radiation solution was not generated. The absorbed radiation for the equilibrium formulation is similar to the nonequilibrium formulation at each of the calculated points. At the 1651-s conditions, the flow is in chemical and thermal equilibrium and all of the formulations produce similar results.

Figure 12 shows a comparison of convective heating along the trajectory for the three formulations. The convective heating for the one-temperature thermal model is similar to the nonequilibrium formulation at each of the calculated points, while the equilibrium formulation is higher. The equilibrium formulation leads to higher convective heating because the accelerated reaction rates result in more atomic recombination in the boundary layer. The release of energy in the boundary layer raises the translational temperature and the convective heating. The increased recombination in the boundary layer is illustrated in Fig. 13, which shows a log–log plot of the mass fractions of N_2, O_2, N, and O near the stagnation

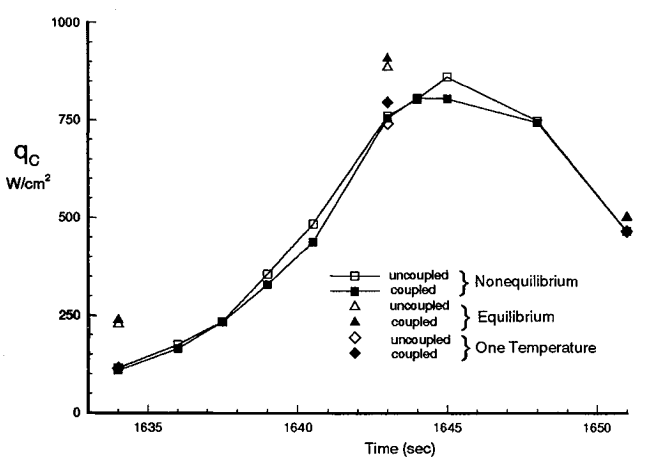

Fig. 12 Effects of thermal and chemical equilibrium on the convective heating along the Fire II trajectory.

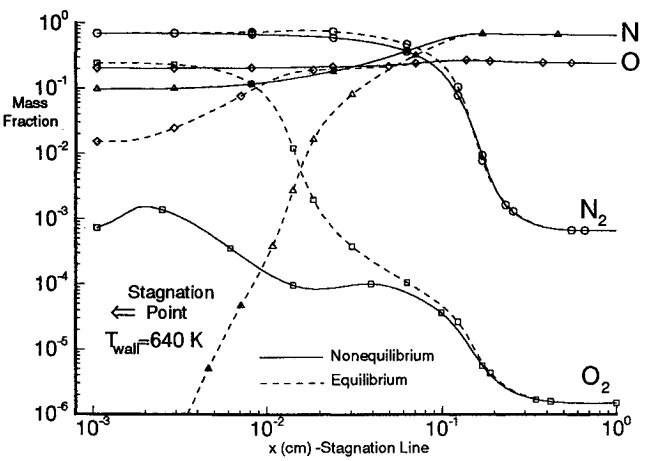

Fig. 13 Mass fractions near the stagnation point for the Fire II-1643-s conditions.

Table 3 Comparison of computational efficiency on a Cray-C90 (50 radiation points)

	Total CPU time, s	Mflops
LORAN	53.43	61.6
NOVAR	8.37	332.8

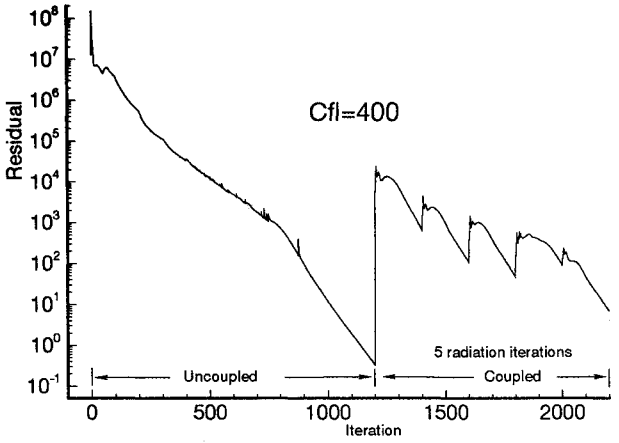

Fig. 14 Convergence history for the Fire II-1639-s calculation.

point at the 1643-s conditions. It can be seen that the flow is close to equilibrium about 1 cm from the wall. Then, the nonequilibrium and equilibrium formulations diverge as the cold wall is approached. Even at the 1651-s conditions, this effect is observed because there is still atomic oxygen present in the boundary layer. More details about these calculations can be found in Ref. 15.

Computational Efficiency

One of the objectives of this study was to develop a tool for the prediction of radiating flowfields that is both accurate and numerically efficient. At the start of this study, timing estimates of the LORAN code indicated that its performance was poor on a vector machine. Since calculating the radiative properties is a large fraction of the total computational cost, an effort was made to improve the computational efficiency of the radiation algorithm, which resulted in the NOVAR code. Table 3 shows the CPU time required to calculate the radiation properties and the radiation transport for 50 points along the stagnation line at the 1634-s conditions. Timing comparisons were performed on a Cray-C90. The present method requires approximately 8 s to perform this calculation. To perform a similar calculation with LORAN required about 53 s. Thus, over a factor of 6 improvement in the computational efficiency has been obtained with the radiation solver developed for this work, NOVAR. The reduced computational time for NOVAR is the result of extensive vectorization and optimization for the Cray-C90 and algorithm modifications to make the method more efficient.

Figure 14 shows a convergence history of the 1639-s calculation for the GIANTS/NOVAR combination. For the first 1200 iterations, GIANTS is run without radiation, then the first radiation solution is generated using NOVAR. GIANTS is then run for 200 flow iterations with the radiation solution fixed. The calculation of a new radiation field and 200 flow iterations constitutes one radiation iteration. Each of the spikes in the residual represent the calculation of a new radiation field. It can be seen that the radiation field is close to converged by the fifth radiation iteration because the calculation of a new radiation solution has only a small effect on the overall residual. The CFL number after the 450th iteration was 400. The CFL number for the flow solver was not lowered when radiation was included in the calculation. In general, it was found that the stability of the flow code was unaffected by radiation coupling for the cases considered in this study. The total CPU time used for this calculation (uncoupled and coupled) was about 2100 s on a Cray-C90. The calculation of the radiation properties required about 20% of the total CPU time.

Concluding Remarks

A nonequilibrium, axisymmetric, Navier–Stokes flow solver with coupled radiation, GIANTS/NOVAR, has been developed for use in the design of thermal protection systems for vehicles where radiation effects are important. The present method was compared with an existing flow and radiation solver and with the Project Fire II experimental data. Excellent agreement was obtained over the entire Fire II trajectory with the experimentally determined values of the stagnation radiation intensity in the 0.2–6.2 eV range and the total stagnation heating.

In comparing with the experimental data, the sensitivity of the numerical simulation to various flow models was examined. From this sensitivity study a number of conclusions can be made about what flow models are needed to accurately simulate the Fire II experiment. A minimum combination of a two-temperature thermal model consisting of a separate translation–rotational temperature and a vibrational temperature was needed to obtain a good agreement with the experimental radiation intensity. It was found that the populations of the various vibrational and electronic states could be characterized by a Boltzmann distribution at the vibrational temperature. Thus, including the electronic energy and solving for a separate electronic temperature was unnecessary. However, employing a one-temperature thermal model was found to be inadequate for simulating the experiment. For trajectory conditions with large thermal nonequilibrium, the one-temperature model overpredicted the experimental stagnation radiation intensity.

To simulate chemical effects, finite rate chemistry with electron impact ionization characterized by the translational temperature provided the best agreement with the experimental data over the entire trajectory. Whether or not this result is fortuitous or due to correct physical modeling is not known at this time. A flow calculation simulating equilibrium conditions was found to overpredict the experimental stagnation heating. The increased heating resulted from excessive atomic recombination in the boundary layer that increased the convective heating.

The computational efficiency of the radiation properties model developed in this work, NOVAR, has been significantly improved over LORAN. The present model was found to be about six times faster than LORAN on a Cray-C90. Finally, the stability of the Navier–Stokes solver, GIANTS was not affected when loosely coupled with radiation.

Acknowledgments

The present research has been supported by a Grant from the National Research Council. Computer time has been provided by the Thermal Protection Materials Branch at NASA Ames Research Center. David Olynick would like to acknowledge some helpful suggestions from Tom Edwards.

References

[1]Park, C., "Calculation of Nonequilibrium Radiation in the Flight Regimes of Aeroassisted Orbital Transfer Vehicles," *Thermal Design of Aeroassisted Orbital Transfer Vehicles*, edited by H. F. Nelson, Vol. 96, Progress in Aeronautics and Astronautics, AIAA, New York, 1985, pp. 395–418.

[2]Candler, G. V., "The Computation of Weakly Ionized Hypersonic Flows in Chemical Nonequilibrium," Ph.D. Dissertation, Stanford Univ., Stanford, CA, June 1988.

[3]Hartung, L. C., Mitcheltree, R. A., and Gnoffo, P. A., "Coupled

Radiation Effects in Thermochemical Nonequilibrium Shock Capturing Flowfield Calculation," AIAA Paper 92-2868, July 1992.

[4]Cornette, E. S., "Forebody Temperatures and Calorimeter Heating Rates Measured During Project Fire II Reentry at 11.35 km/s," NASA TM X-1305, Nov. 1966.

[5]Gnoffo, P. A., Gupta, R. N., and Shinn, J. L., "Conservation Equations and Physical Models for Hypersonic Air Flows in Thermal and Chemical Nonequilibrium," NASA TP-2867, Feb. 1989.

[6]Park, C., *Nonequilibrium Hypersonic Aerothermodynamics*, Wiley, New York, 1990.

[7]Lee, J.-H., "Basic Governing Equations for the Flight Regimes of Aeroassisted Orbital Transfer Vehicles," *Thermal Design of Aeroassisted Orbital Transfer Vehicles*, edited by H. F. Nelson, Vol. 96, Progress in Astronautics and Aeronautics, AIAA, New York, 1985, pp. 3–53.

[8]Candler, G. V., and MacCormack, R. W., "The Computation of Hypersonic Ionized Flows in Chemical and Thermal Nonequilibrium," *Journal of Thermophysics and Heat Transfer*, Vol. 5, No. 3, 1991, pp. 266–273.

[9]Millikan, R. C., and White, D. R., "Systematics of Vibrational Relaxation," *Journal of Chemical Physics*, Vol. 39, No. 12, 1963, pp. 3209–3213.

[10]Park, C., "Review of Chemical-Kinetic Problems of Problems of Future NASA Missions, I: Earth Entries," *Journal of Thermophysics and Heat Transfer*, Vol. 7, No. 3, 1993, pp. 385–398.

[11]Wilson, J., "Ionization Rates of Air Behind High Speed Shock Waves," *Physics of Fluids*, Vol. 9, No. 10, 1966, pp. 1913–1921.

[12]Gupta, R. N., Yos, J. M., Thompson, R. A., and Lee, K., "A Review of Reaction Rates and Thermodynamic and Transport Properties for an 11-Species Air Model for Chemical and Thermal Nonequilibrium Calculations to 30,000 K," NASA RP-1232, Aug. 1990.

[13]Stallcop, J., private communication, Computational Chemistry Branch, NASA Ames Research Center, Moffett Field, CA, 1993.

[14]Bartlett, E. P., Kendal, R. M., and Rindal, R. A., "An Analysis of the Coupled Chemically Reacting Boundary Layer and Charring Ablator: Part IV-A Unified Approximation for Mixture Transport Properties for Multicomponent Boundary-Layer Applications," NASA CR-1063, June 1968.

[15]Olynick, D. R., Henline, W. D., Chambers, L. H., and Candler, G. V., "Comparisons of Coupled Radiative Navier-Stokes Flow Solutions with the Project Fire II Flight Data," AIAA Paper 94-1955, June 1994.

[16]Gökçen, T., "Computation of Nonequilibrium Radiating Shock Layers," AIAA Paper 93-0144, Jan. 1993.

[17]Hartung, L. C., "Development of a Nonequilibrium Radiative Prediction Method for Coupled Flowfield Solutions," *Journal of Thermophysics and Heat Transfer*, Vol. 6, No. 4, 1992, pp. 618–625.

[18]Hartung, L. C., "Nonequilibrium Radiative Heating Prediction Method for Aeroassist Flowfields with Coupling to Flowfield Solvers," Ph.D. Dissertation, North Carolina State Univ., Raleigh, NC, 1991.

[19]Park, C., "Assessment of a Two-Temperature Kinetic Model for Ionizing Air," *Journal of Thermophysics and Heat Transfer*, Vol. 2, No. 3, 1989, pp. 233–244.

[20]Park, C., "Nonequilibrium Air Radiation (NEQAIR) Program: User's Manual," NASA TM 86707, July 1985.

[21]Greendyke, R. B., and Hartung, L. C., "A Convective and Radiative Heat Transfer Analysis for the Fire II Forebody," AIAA Paper 93-3194, July 1993.

[22]Gally, T. A., and Carlson, L. A., "An Approximate Local Thermodynamic Nonequilibrium Radiation Model for Air," AIAA Paper 92-2972, July 1992.

[23]Stewart, D., private communication, Thermal Protection Branch, NASA Ames Research Center, Moffett Field, CA, 1993.

[24]Cauchon, D. L., "Radiative Heating Results from the Fire II Flight Experiment at Reentry Velocity of 11.4 Km/s," NASA TM X-1402, July 1967.

[25]Cauchon, D. L., Mckee, C. W., and Cornette, E. S., "Spectral Measurements of Gas-Cap Radiation During Project Fire Flight Experiments at Reentry Velocities Near 11.4 Kilometers Per Second," NASA TM X-1389, Oct. 1967.

[26]Olynick, D. R., "A New LU-SGS Flow Solver for Calculating Reentry Flows," Ph.D. Dissertation, North Carolina State Univ., Raleigh, NC, Dec. 1992.

[27]Nicolet, W. E., "Rapid Methods for Calculating Radiation Transport in the Entry Environment," NASA CR-2528, April 1975.